Semiclosed Loop Based on Predictive Current Control for SPMSM Drives During Servo Stamping

Qi Li, *Graduate Student Member, IEEE*, Yan Lv, Ralph Kennel, *Senior Member, IEEE*, and Jose Rodriguez, *Life Fellow, IEEE*

***Abstract*—Nonlinear factors in the industrial servo press currently, including mechanisms for force amplification, installed clearances, gears backlash, and variations in rotational inertia, are commonly not considered during the control process. They would impact the control accuracy of the actuator's crank and slide and even affect the quality of material forming. So, the conventional linear control method, field-oriented control based on the miniclosed loop of the electrical machine position utilizing kinematics, cannot follow the trajectory smoothly and accurately. This study proposes a solution to address these issues by introducing a semiclosed loop control approach. This method fully accounts for the Lagrangian approach for the dynamic model of the servo press. The torque reference of the computed torque algorithm is implemented by model predictive current control. A comprehensive and comparative trial and analysis of the impacts of critical parameters are conducted. The proposed method is practically tested on a 1600-kN press equipped with a dual-core DSP servo drive. Experimental results demonstrate the effectiveness of this control approach, which significantly enhances the control accuracy of crank position and speed while also reducing the switching frequency and losses of the servo press drive.**

***Index Terms*—Lagrangian approach, predict current control, semiclosed loop, servo press drive.**

I. Introduction

THE advancement of material technology has led to the emergence of several challenges in sheet metal forming, including the utilization of high-strength materials, achieving high precision, and dealing with low ductility [1]. Servo presses have demonstrated successful application in difficult-to-form materials, such as high-strength steel, aluminum alloy, and magnesium alloy [2]. Servo presses have gained considerable interest in stamping workshops due to their ability to extend mold life, increase productivity, reduce noise, save energy, and achieve high productivity [3]. The transmission exhibits a simple structure [4]. The servo press is powered by the servo electrical machine and removes the mechanical flywheel, clutch, and brake.

The primary attribute of servo stamping is the highly flexible motion of the slide. The slide's motion can be adjusted using programmable and numerical curves. The slide velocity can be adjusted to a lower speed during the stamping process and increased to a higher speed during the idle run. [5]. Furthermore, the slide can dwell or reverse at any point in the stroke. The stamping product type determines the servo press's motion curve, which, in turn, impacts forming speed, spring-back alteration, production efficiency, and product quality.

The control for the press can be classified into two control loops: 1) a miniclosed loop and 2) a semiclosed loop. The miniclosed-loop method relies on the position feedback of the electrical machine. The assumption of the miniclosed loop is the ideal condition that the inertia is constant and the position relationship between the crank and electrical machine is linear. Gao et al. [6] proposed the cascaded structure of field-oriented control (FOC) for a two-sided output permanent magnet synchronous machine (PMSM) integrated with planetary gear in the servo press. Lu et al. [7] adopted the Luenberger observer to estimate the load torque and implemented feed-forward compensation to improve the speed control performance on the press. Hybrid model predictive current control (MPC), combining predictive torque control (PTC) with generalized predictive control was also developed to predict long horizons of machine speed in the servo mechanical press [8].

Clearances in kinematic joints are inevitable in transmission assemblies due to factors, such as machining accuracy, friction, and wear [9]. Clearances could reduce machining accuracy, decrease the service life of mechanical systems, and even damage parts [10]. Conventional spur gear drives lack the ability to achieve nonbacklash operation in machines [11]. Furthermore, the interaction between the components in the drive line may lead to an increase in vibration amplitude [12]. So, there exists a discrepancy between the expected and actual motion [13]. In addition, excessive error causes unexpected defects, such as surface cracks and wrinkles during stamping. It is critical to improve the accuracy of motion as much as possible, which is also the aim of this article.

Manuscript received 22 August 2023; revised 21 January 2024 and 9 April 2024; accepted 18 May 2024. Date of publication 24 May 2024; date of current version 16 July 2024. This work was supported by the Taishan Industrial Leading Talents Project Special Fund. An earlier version of this paper was presented at the 2023 IEEE International Conference on Predictive Control of Electrical Drives and Power Electronics (PRECEDE) on Jun. 18, 2023, in Wuhan, China [DOI: 10.1109/PRECEDE57319.2023.10174607]. Recommended for publication by Associate Editor D. Zhang. *(Corresponding author: Qi Li.)*

Qi Li and Ralph Kennel are with the Institute for Electrical Drive Systems and Power Electronics, Technical University of Munich (TUM), 80333 Munich, Germany (e-mail: qi.li2@tum.de; ralph.kennel@tum.de).

Yan Lv is with the Jining Keli Photoelectronic Industrial Company, Ltd., Jining 100124, China (e-mail: lihaiming@sdkeli.com).

Jose Rodriguez is with the University San Sebastian in Santiago, Santiago 20014, Chile (e-mail: jose.rodriguezp@uss.cl).

Color versions of one or more figures in this article are available at https://doi.org/10.1109/TPEL.2024.3405413.

Digital Object Identifier 10.1109/TPEL.2024.3405413

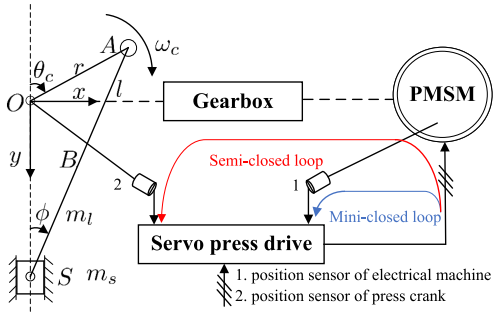

Fig. 1. Slide–crank mechanism of the servo press.

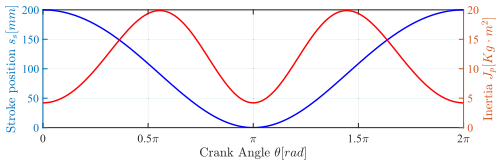

Fig. 2. Variable inertia and stroke position relationship with a crank angle.

There is a typical mechanism of the crank–slide press in Fig. 1. With the crank angle varying, the inertia of the whole press system changes in Fig. 2. When the crank rotates in one direction, the stroke position is nonlinear with the crank angle in Fig. 2. To our knowledge, few studies have yielded that a semiclosed loop is proposed to solve the nonlinear mechanical problem considering the variable inertia and clearances.

A moving horizon estimator is presented to use the estimated inertia moment to improve the robust performance [14]. The model reference adaptive system is used to identify the moment of inertia online [15]. The inertia identification is adopted to get an accurate inertia observation result [16].

Based on the accurate torque model of ball-screw, the full-closed-loop position control structure is established for high-precision control [17], [18]. A dynamic error modeling method for elastic joints with cascade control is built, allowing the revelation of influence on dynamic errors [19].

Researchers have explored the possibility of solving the accuracy problem in the alternative pathway from the crank position by implementing a semiclosed-loop control. It employed a position sensor mounted on the crank as feedback. The reference and actual positions of the crank are directly utilized in the semiclosed-loop control. Consequently, the semiclosed loop is beneficial for enhancing the accuracy of the crank position control, particularly when clearance is present. A one-step MPC strategy based on a backpropagation neural network is proposed for the precise forging processes [20]. Another study derives a dynamic model by the Lagrange approach for a servo crank press machine [21]. MPC of an induction machine with a computed torque was described to meet the positioning requirement in a servo press [22]. The authors in [23] and [24] developed the Lagrangian approach to create a dynamical model to increase the accuracy of position.

However, rare studies focused much attention on the crank's precision and comparative experiment to validate the control approach. Meanwhile, previous research on this strategy has primarily focused on the press perspective, overlooking the significance of key control parameters. The research with regard to dynamical performances and complicated states of electrical machines and drives is also even less.

In the realm of electrical drives, two widely employed strategies for control are FOC and direct torque control. In recent years, the advancement of processors has garnered significant attention on MPC from scholars in the pursuit of enhancing the current and torque performances of machines [25], [26]. This has led to a particular emphasis on MPC techniques, such as deadbeat control (DB), PTC [27], predictive current control (PCC) [28], [29], among others [30]. Finite control set (FCS) PCC has been focused on in recent years due to its ability to achieve desirable current performance and faster dynamic behavior [30], [31]. The FCS-PCC algorithm has been shown to not require the utilization of a weighting factor for the dq current track, as demonstrated in previous research [32]. The achievement of high controller bandwidth is made possible in PCC due to the absence of internal current loops. Numerous investigations have been conducted to elucidate the MPC algorithm's application in the realm of electrical drive systems, with a particular focus on current control and speed control strategies. Consequently, the control strategy based on MPC can be categorized into two distinct approaches: 1) model predictive direct speed control [33], [34] and 2) cascaded predictive speed control [35]. In the study, Zhang et al. [28] present a comprehensive analysis of a hybrid vector MPC strategy. The primary objective of another approach is to enhance the optimization of the output voltage [33]. The proposed methodology for the design of the cascaded band control-based PCC is presented in this approach. In contrast to existing approaches, the proposed method eliminates a weighting factor, thereby reducing the computational burden associated with the control system [35]. The utilization of MPC not only yields superior control performance but also facilitates a reduced switching frequency.

The key innovations in this article are as follows.

1) Utilizing the dynamic model of a press machine and the crank position sensor, a control method based on semi-closed loop control is proposed, achieving an order of magnitude improvement in the precision of crank position and speed control.
   The following surpasses the innovation presented in the original conference papers.
2) The global stability issue of the computed torque algorithm is demonstrated.
3) Experimental verification is employed to investigate the impact of control parameters and high bandwidth in the computed torque method on the precision of crank position and speed control.
4) Leveraging the advantages of predictive control for a faster current response, a combined approach of computed torque and FCS-PCC is introduced to reduce the switching frequency.
5) The validation is done on a dual-core DSP using a servo driver developed through authentic research, not in a hardware-in-the-loop or prototype system. Comparative experiments under no-load and heavy-load conditions are carried out to analyze the results on an industrial servo press machine.

II. Lagrangian Approach for Dynamic Model of Servo Press

A typical slide–crank press mechanism with a capability of 1600 kN driven by a PMSM is selected in this study. Fig. 1 shows the mechanism's physical symbols. The crank radius, the rod length, and the ratio of the gearbox are denoted by $r = 100$ mm, $l = 580$ mm, and $n = 48.899$, respectively. m_l and m_s represent the mass of link and slide, respectively. J_c is the inertia of the crank. The mass center of the connecting rod is at midpoint B. The initial position is denoted as top dead center (TDC) while the position where the servo press exerts its maximal force is designated as bottom dead center (BDC). The angles of clockwise rotation are defined as θ_c and ϕ in Fig. 1, respectively. ω_c is the angular speed of the press crank. PMSM is amplified by the transmission of a gearbox, and the slide can move up and down along the guides. The gearbox includes the two-level reducer and the other one-level big ratio reducer.

$$x_A = r\sin\theta_c, y_A = -r\cos\theta_c, x_S = 0, \frac{\sin\phi}{r} = \frac{\sin(\pi-\theta_c)}{l}$$
$$y_S = l\cos\phi - r\cos\theta_c, x_B = \frac{x_A + x_S}{2}, y_B = \frac{y_A + y_S}{2}. \quad (1)$$

The dynamic model of the servo press mechanism is derived by the Lagrangian approach. The Lagrangian equation demonstrates the difference between kinetic energy E_k and potential energy E_p. Because the slide–crank mechanism is a single-DOF system, the independent generalized coordinate is considered. In this study, the generalized force τ_c is designated as the torque acting on the crank while the generalized variable θ_c is defined as the crank angle. The Lagrange equation is described as

$$\frac{d}{dt}\left(\frac{\partial\Gamma}{\partial\dot{\theta_c}}\right) - \frac{\partial\Gamma}{\partial\theta_c} = \tau_c \quad (2)$$

where the Lagrangian is the difference between the kinetic and potential energies, $\Gamma = E_k - E_p$. Given the compensation of transmission gravity by the balancer, we can assume that the potential energy E_p is equal to zero. The kinetic energy of the slide–crank mechanism can be determined by summing the individual energies involved

$$E_k = E_c + E_l + E_s + E_m \quad (3)$$

where E_c, E_l, E_s, and E_m are the crank kinetic energy, the connecting rod kinetic energy, the slide kinetic energy, and the machine and gearbox kinetic energy, respectively.

The crank is primarily concerned with a rotational motion. The connecting rod exhibits both rotational and translation motion. The slide solely encompasses translation motion. Therefore, we have

$$E_c = \frac{1}{2}J_c\dot{\theta_c}^2, \quad E_m = \frac{1}{2}J_g(\omega_m/n)^2$$
$$E_l = \frac{1}{2}J_l\dot{\phi}^2 + \frac{1}{2}m_l v_l^2, \quad \dot{\phi} = \frac{r\dot{\theta_c}\cos\theta_c}{\sqrt{l^2 - r^2\sin^2\theta_c}}$$
$$v_l^2 = \left(\frac{1}{2}r\dot{\theta_c}\cos\theta_c\right)^2 + \left(r\dot{\theta_c}\sin\theta_c - \frac{1}{2}l\dot{\phi}\cos\phi\right)^2$$

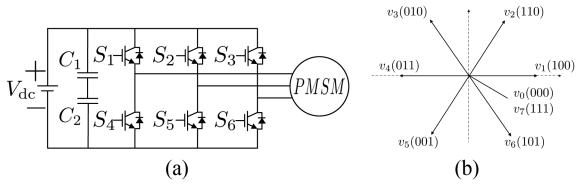

Fig. 3. (a) Two-level voltage source inverter. (b) Voltage vectors.

$$E_s = \frac{1}{2}m_s v_s^2, \quad v_s^2 = \left(l\dot{\phi}\sin\phi + r\dot{\theta_c}\sin\theta_c\right)^2 \quad (4)$$

where J_l is the rotatory inertia of connecting rod rotating around point S; v_l is the speed of mass centers of the link; v_s is the speed of slide; ω_m is the angular speed of electrical machine; J_g is the inertia of electrical machine and gearbox from the side of the crank.

By substituting the Lagrange equation (2) with kinetic energy (4), the dynamic model of the servo press can be simplified in the following equation:

$$M(\theta_c)\ddot{\theta_c} + N(\theta_c)\dot{\theta_c}^2 = \tau_c. \quad (5)$$

Herein, the slide–crank inertia matrix $M(\theta_c)$ is given, and $N(\theta_c)$ is the centrifugal matrix with respect to $M(\theta_c)$.

III. Control Schemes for Servo Press Drive

A. Predictive Current Control

A well-known set of equations in synchronously rotating reference coordinates describes surface-mounted PMSM (SPMSM). The stator voltage equations are

$$v_d = R_s i_d + L_d\frac{di_\mathrm{d}}{dt} - \omega_e L_q i_q$$
$$v_q = R_s i_q + L_q\frac{di_q}{dt} + \omega_e L_d i_d + \omega_e\psi_f \quad (6)$$

where v_d, v_q, i_d, and i_q are the dq-axis voltages and currents in the rotating frame, respectively; R_s is the stator resistance; ω_e is the electrical angular speed; ψ_f is the flux of permanent magnet; L_d and L_q are the dq-axis stator flux, respectively.

The mechanical model of PMSM can be obtained as follows:

$$T_\mathrm{e} = \frac{3}{2}p\left[\psi_\mathrm{f} i_\mathrm{q} + (L_\mathrm{d} - L_\mathrm{q})\, i_\mathrm{d} i_\mathrm{q}\right] = J\dot{\omega}_\mathrm{m} + B_\mathrm{r}\omega_\mathrm{m} + T_\mathrm{L} \quad (7)$$

where B_r is the friction constant, J is the inertia constant, and ω_m is the mechanical angular velocity. T_e and T_L are the electrical torque and load torque, respectively.

The two-level three-phase inverter comprises six nonzero-voltage vectors ($v_1, v_2, \ldots, v_6$) and two zero-voltage vectors (v_0 and v_7), as depicted in Fig. 3. The stator voltages in the two-level voltage source inverter can be expressed in the stationary and synchronously rotating reference coordinates

$$\begin{bmatrix} v_\mathrm{a} \\ v_\mathrm{b} \\ v_\mathrm{c} \end{bmatrix} = \frac{V_\mathrm{dc}}{3}\begin{bmatrix} 2 & -1 & -1 \\ -1 & 2 & -1 \\ -1 & -1 & 2 \end{bmatrix}\begin{bmatrix} S_1 \\ S_2 \\ S_3 \end{bmatrix}$$

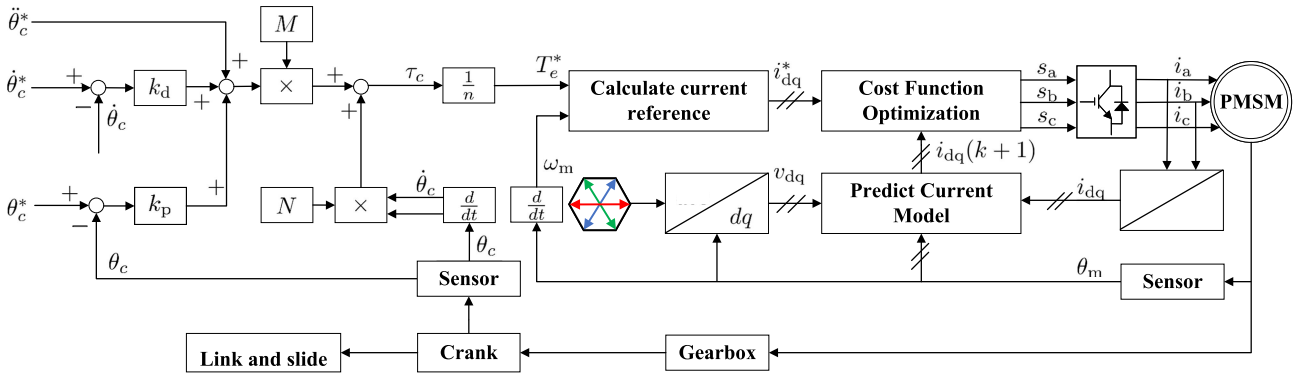

Fig. 4. Proposed control algorithm.

$$\begin{bmatrix} v_\alpha \\ v_\beta \end{bmatrix} = \begin{bmatrix} 1 & -\frac{1}{2} & -\frac{1}{2} \\ 0 & \frac{\sqrt{3}}{2} & -\frac{\sqrt{3}}{2} \end{bmatrix} \begin{bmatrix} v_\mathrm{a} \\ v_\mathrm{b} \\ v_\mathrm{c} \end{bmatrix}$$
$$\begin{bmatrix} v_\mathrm{d} \\ v_\mathrm{q} \end{bmatrix} = \frac{2}{3} \begin{bmatrix} \cos(\theta_\mathrm{e}) & \sin(\theta_\mathrm{e}) \\ -\sin(\theta_\mathrm{e}) & \cos(\theta_\mathrm{e}) \end{bmatrix} \begin{bmatrix} v_\alpha \\ v_\beta \end{bmatrix} \quad (8)$$

where v_α and v_β are the voltages in the stator reference frame, v_a, v_b, and v_c are the phase voltages of PMSM, respectively. θ_e is the electrical angle.

The d-axis reference current $i_\mathrm{d} = 0$ is an appropriate control method for SPMSM.

Since the control method is implemented on a digital microcontroller, a time delay issue exists. Fig. 4 shows the best candidate voltage vector selected by the cost function at the sampling k instant, available at the next $k+2$ control period. The forward Euler approximation in discrete time gives the calculation delay compensated current

$$i_d(k+1) = \left(1 - \frac{R_s T_s}{L_d}\right) i_d(k) + \frac{w_e L_q T_s}{L_d} i_q(k) + \frac{T_s}{L_d} v_d(k)$$
$$i_q(k+1) = \left(1 - \frac{R_s T_s}{L_q}\right) i_q(k) - \frac{w_e L_d T_s}{L_q} i_d(k) + \frac{T_s}{L_q} v_q(k) - \frac{\omega_e \psi_f}{L_q}. \quad (9)$$

These compensated currents $i_d(k+1)$ and $i_p(k+1)$ substitute the measured current $i_d(k)$ and $i_q(k)$ to predict the next $k+2$ current as

$$i_d(k+2) = \left(1 - \frac{R_s T_s}{L_d}\right) i_d(k+1) + \frac{w_e L_q T_s}{L_d} i_q(k+1) + \frac{T_s}{L_d} v_d(k+1)$$
$$i_q(k+2) = \left(1 - \frac{R_s T_s}{L_q}\right) i_q(k+1) - \frac{w_e L_d T_s}{L_q} i_d(k+1) + \frac{T_s}{L_q} v_q(k+1) - \frac{\omega_e \psi_f}{L_q}. \quad (10)$$

The cost function of MPC for the next $k+2$ instant is the optimization of a control law with the following structure:

$$J = |i_q^*(k+2) - i_q(k+2)| + |i_d^*(k+2) - i_d(k+2)| \quad (11)$$

where $i_d^*(k+2)$ and $i_q^*(k+2)$ represent the rotating frame's dq-axis reference currents, where k denotes the index of the stator voltage vector used to calculate the predictions $i_q(k+2)$ and $i_d(k+2)$, respectively. The current reference is externally generated by the computed torque algorithm.

Ultimately, the optimization process is executed, wherein the inverter-voltage vector that minimizes the cost function is chosen as the best switching state for the subsequent sampling instant $k+2$.

B. Computed Torque for Servo Press

Computed torque control linearizes and decouples press dynamics using a dynamic model, so other well-developed linear control algorithms can regulate press motion. The computed torque includes closed-loop crank position and force control.

As a semiclosed-loop control mechanism, the computed torque uses a crank position sensor for position feedback. The torque calculation takes press inertia, mass, and kinematics into account. The semiclosed-loop control objects are crank position and speed. Thus, it improves crank position precision as much as feasible.

Improving control law tracking can be achieved by introducing state feedback in Fig. 4. The linear equation (5) suggests the control law

$$M(\theta_c)\left(\ddot{\theta}_c^{\,*} + k_d\dot{e} + k_p e\right) + N(\theta_c)\dot{\theta}_c^{\,2} = \tau_c \quad (12)$$

where $e = \theta_c^* - \theta_c$, and k_d and k_p are constant gains.

When substituted in (2), the error dynamics can be written as

$$M\left(\ddot{e} + k_d\dot{e} + k_p e\right) = 0. \quad (13)$$

Since M is always positive definite, we have

$$\ddot{e} + k_d\dot{e} + k_p e = 0. \quad (14)$$

The equation presented here describes the error between the actual and the reference trajectories. Therefore, when the initial

TABLE I
PARAMETERS FOR ELECTRICAL MACHINES

Symbol	Quantity	Value
P_{nom}	nominal power	28.26 kW
i_s	nominal current	55.79 A
$\cos(\varphi)$	power factor	0.82
ω_{nom}	nominal speed	1000 r/min
p	number of pole pairs	4
R_s	stator resistance	0.169Ω
$L_d = L_q$	inductance	7.07 mH
J_m	inertia of machine	0.041 kg.m^2

angle and velocity of the crank align with the reference angle and speed, the crank will accurately trace the intended trajectory.

The error dynamics can be written as a first-order linear system

$$\frac{\mathrm{d}}{\mathrm{d}t}\begin{bmatrix} e \\ \dot{e} \end{bmatrix} = \underbrace{\begin{bmatrix} 0 & 1 \\ -k_p & -k_d \end{bmatrix}}_{A}\begin{bmatrix} e \\ \dot{e} \end{bmatrix}. \tag{15}$$

It suffices to show that each of the eigenvalues of A has a negative real part. Let $\lambda \in \mathbb{C}$ be an eigenvalue of A. Then

$$\begin{aligned} |A - \lambda I| &= \begin{vmatrix} 0 & 1 \\ -k_p & -k_d \end{vmatrix} - \lambda I = \begin{vmatrix} -\lambda & 1 \\ -k_p & -k_d - \lambda \end{vmatrix} \\ &= \lambda^2 + k_d\lambda + k_p = 0, k_d, k_p > 0 \end{aligned} \tag{16}$$

and, hence, the real part of λ is negative. Above is the proof of the global stability of the computed torque control law.

IV. SIMULATION AND EXPERIMENT

The parameters of SPMSM applied to the 1600-kN servo press are listed in Table I. The proposed algorithm is developed and validated in MATLAB-Simulink software and on a servo press.

A. Simulation

The proposed algorithm is designed in the MATLAB function.The simulation for the proposed algorithm is done under unloaded conditions. The reference and feedback profiles of the crank position, the reference and measured speed, the position error and the speed error, the inertia matrix, and the centrifugal matrix are presented in the first part of Fig. 5. The measured speed of the machine, the reference and measured direct currents, the reference and measured quadrature currents, and the reference electromagnetic torque are presented in the second part of Fig. 5.

At the initial time, a speed reference of 0 r/min at TDC is provided. Then, the SPMSM accelerates to the rated speed. At the crank angle position with 2 rad, the crank speed starts to decelerate to the 70% rated speed. Close to the clamping position with 2.63 rad, the crank speed approaches 30% rated speed to reduce the noise of mold collision. When the crank angle

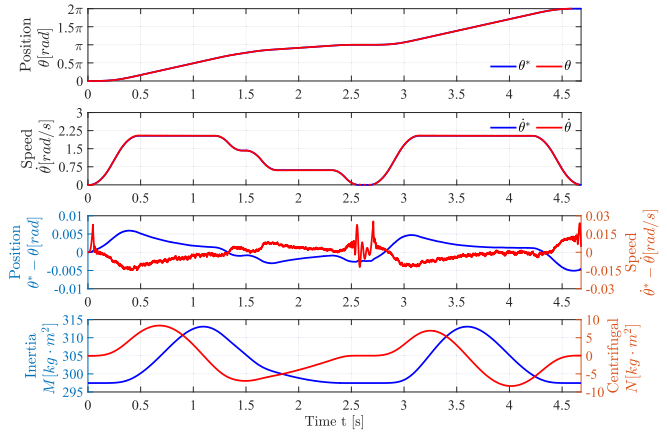

(a)

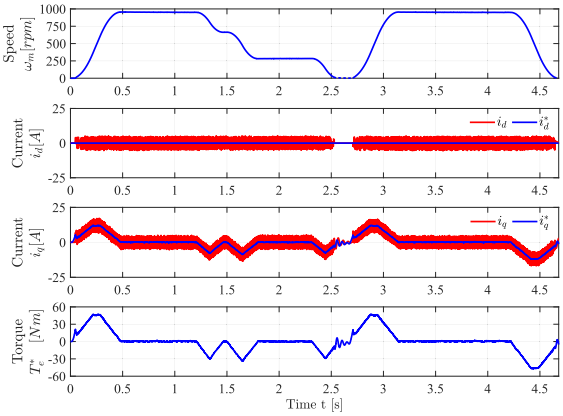

(b)

Fig. 5. Simulation results of the proposed method. (a) Response of the crank. (b) Response of PMSM.

continues to rotate to BDC π rad, it keeps steady and stands still. The dwell time is 0.1 s. After that, it returned to TDC as soon as possible in the first part of Fig. 5. The actual dq-axis current of the proposed algorithm can track the reference current because the PCC method works well to make the current response fast. This simulation demonstrates that the proposed algorithm for the nonlinear position control in servo presses is effective.

B. Experiment

The algorithms proposed in this study are practically implemented in the electrical drive system of an industrial 1600-kN servo press in Fig. 10. The drive system is built around the dual-core microcontroller TMS320F28379D from Texas Instruments Incorporated. The crank and SPMSM utilize the position sensor with Tamagawa resolvers. A nitrogen spring is employed as the load during press load testing, exerting force on the press slide. The experimentation process is categorized into two phases: 1) unloaded and 20 heavy-load press tests. The experimental curves replicate the simulation process. For comparison, the cascaded structures P + PI + PI + FOC and P + DB + PCC are introduced in the miniclosed loop. The DB is the predictive speed approach to track the speed reference with high bandwidth [36]. In the cascaded scheme, the value of position loop parameter P

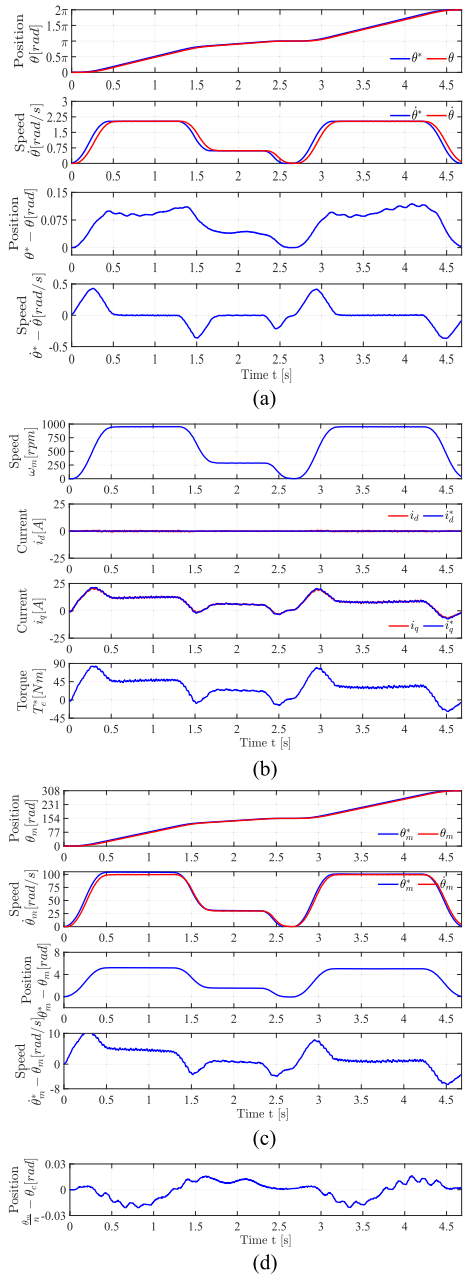

Fig. 6. Experimental results of miniclosed-loop FOC without the load. (a) Response of the crank. (b) Electrical response of PMSM. (c) Mechanical response of PMSM. (d) Error of clearance.

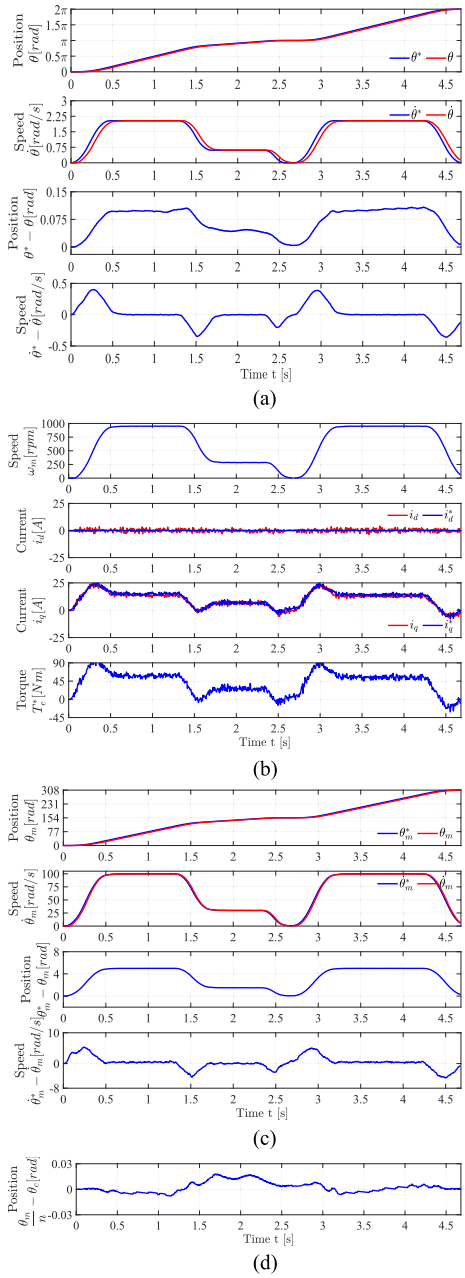

Fig. 7. Experimental results of miniclosed loop DB-PCC without the load. (a) Response of the crank. (b) Electrical response of PMSM. (c) Mechanical response of PMSM. (d) Error of clearance.

is configured as 20, and the speed loop parameters P and I are configured as 2 and 0.8, respectively. Furthermore, the current loop parameters P and I are set to 14 and 1200, respectively. The well-established position control parameter k_p within the semiclosed loop is widely recognized. In this study, particular emphasis is placed on contrasting the influence of a distinct speed control parameter k_d on press crank precision and machine performance. To this end, two separate semiclosed-loop experiments with the same position control parameter $k_p = 300$ have been devised, each employing a distinct k_d parameter, 40 and 70, respectively.

In both experimental trials, Figs. 6(a), 7(a), 8(a), 9(a), 11(a), 12(a), 13(a), and 14(a) illustrate the profiles of crank reference and feedback position, the crank reference and measurement speed, as well as the errors in position and speed. Figs. 6(b), 7(b), 8(b), 9(b), 11(b), 12(b), 13(b), and 14(b) depict the measured speed, the reference and measured dq currents, and the reference electromagnetic torque of the electrical machine. Figs. 6(c) and 7(c) describe the mechanical response of PMSM under unload conditions, including the profiles of machine's reference and feedback position, the machine reference and feedback speed, and errors in machine position and speed. Figs. 6(d) and 7(d) show the errors caused by the clearance of transmissions between PMSM and press crank.

In the four sets of experiments under no-load conditions, the performance of semiclosed-loop control with $k_d = 70$ exhibits

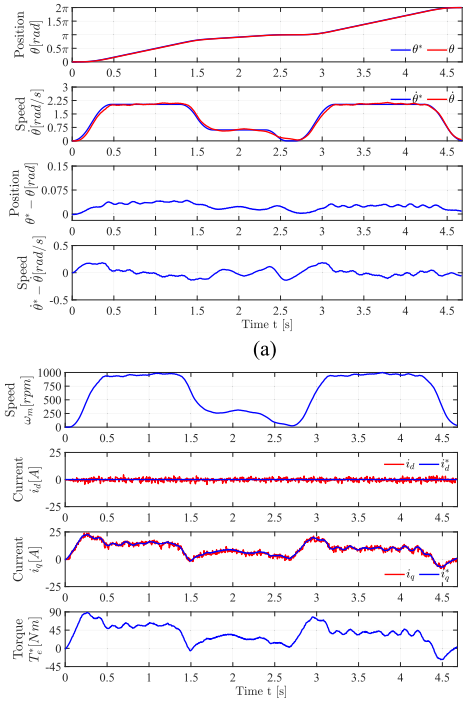

Fig. 8. Experimental results of semiclosed loop $k_d = 40$ without the load. (a) Response of the crank. (b) Response of the PMSM.

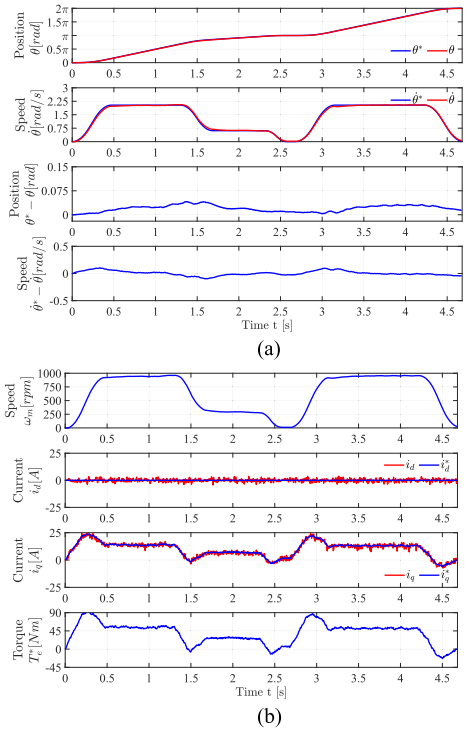

Fig. 9. Experimental results of the semiclosed loop $k_d = 70$ without the load. (a) Response of the crank. (b) Response of PMSM.

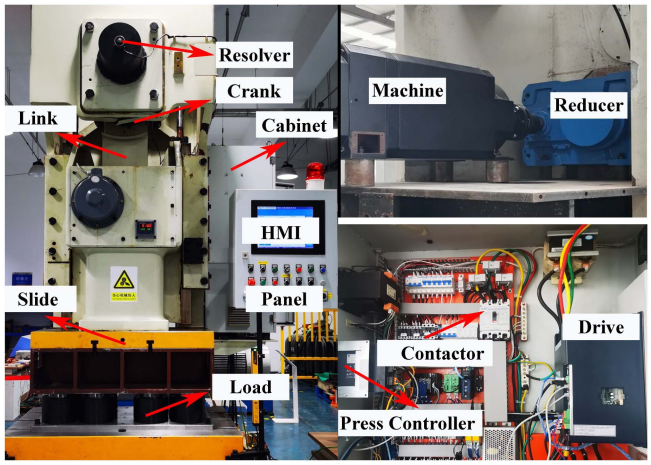

Fig. 10. Test bench of 1600-kN servo press.

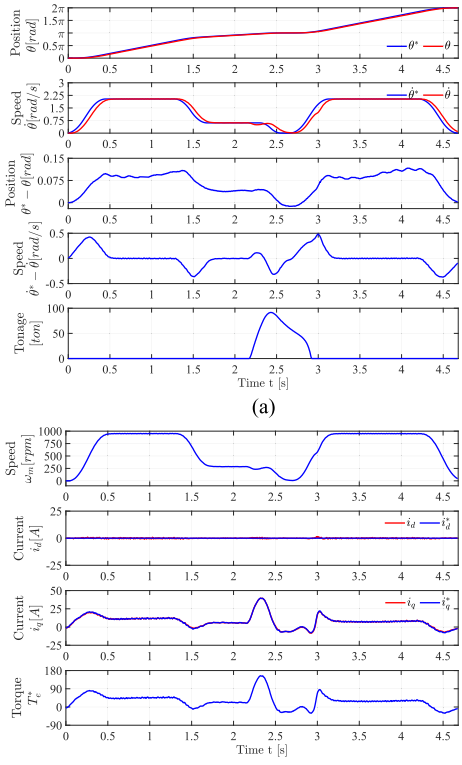

Fig. 11. Experimental results of miniclosed-loop FOC with load impact. (a) Response of the crank. (b) Response of PMSM.

the best trajectory tracking capability, as shown in Table II. The crank position and speed-tracking errors are minimized, and the control precision of both position and speed-tracking errors in Figs. 8(a) and 9(a) is improved by an entire order of magnitude compared to the miniclosed loop control in Figs. 6(a) and 7(a). It is evident that the proposed semiclosed-loop control algorithm demonstrates a significant improvement in press accuracy over the traditional miniclosed-loop control algorithm in Table II.

The unloaded experiments in Figs. 6(c) and 7(c) and Table II show that the mechanical response of PMSM with DB-PCC has

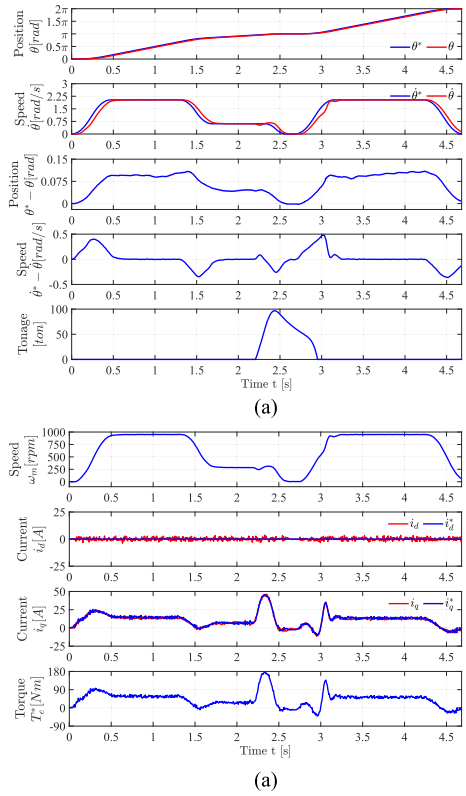

Fig. 12. Experimental results of miniclosed-loop DB-PCC with load impact. (a) Response of the crank. (b) Response of PMSM.

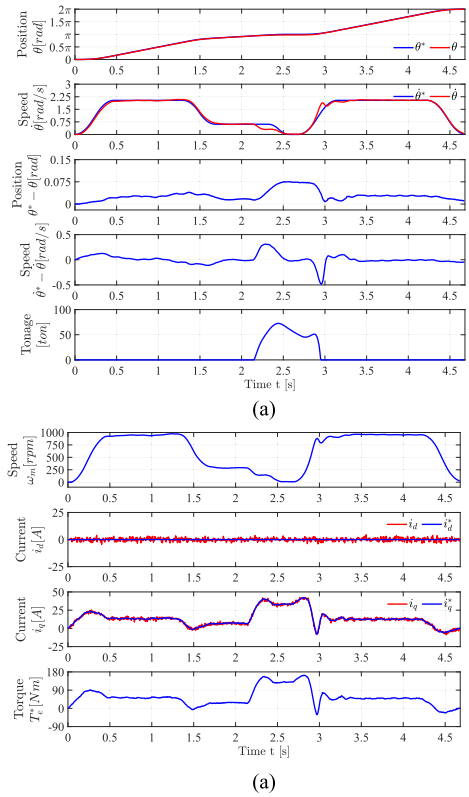

Fig. 13. Experimental results of the semiclosed loop $k_d = 40$ with load impact. (a) Response of the crank. (b) Response of PMSM.

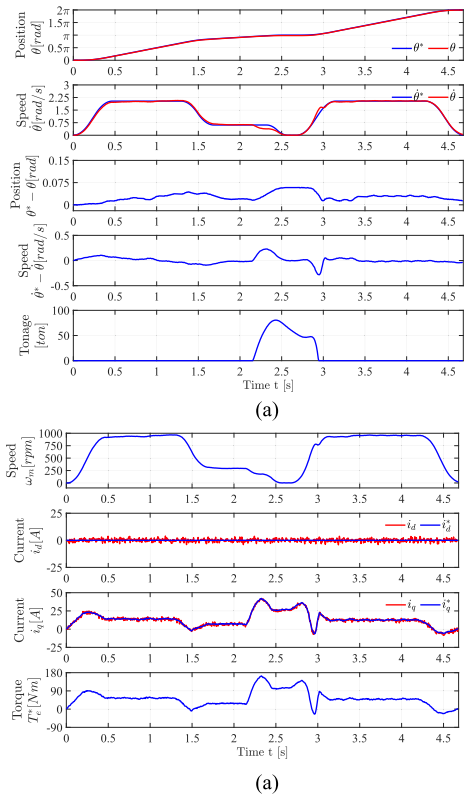

Fig. 14. Experimental results of the semiclosed loop $k_d = 70$ with load impact. (a) Response of the crank. (b) Response of PMSM.

TABLE II
MAXIMUM ERRORS IN THE UNLOAD EXPERIMENTS

	Noload condition			
	miniclosed FOC	miniclosed DB-PCC	semiclosed k_d=40	semiclosed k_d=70
$[\text{rad}]$ $\theta_c^* - \theta_c$	0.1189	0.1081	0.0426	0.0411
$[\text{rad}/s]$ $\dot{\theta}_c^* - \dot{\theta}_c$	0.4290	0.4015	0.1825	0.1015

superior to that of FOC. The obvious advantage of DB-PCC is better speed-tracking performance due to the high bandwidth of the outer loop. However, the more ripple of the q-axis current reference with DB-PCC also occurs accompanied with it in Fig. 7(b).

Analyzing the results concerning machine speed, q-axis current, and electromagnetic torque, it can be observed that the semiclosed-loop algorithm with $k_d = 40$ still exhibits minor fluctuations, especially during the constant speed in Fig. 8(b). This is attributed to the presence of clearances and backlash in the semiclosed-loop control algorithm for the press machine. Although the semiclosed-loop control algorithm is effective and enhances precision, the existence of clearances and backlash leads to minor errors during the tracking process, which, in turn, affects the fluctuations in the inner current control loop. However, when $k_d = 70$, as the tracking error is reduced to a certain extent, the control impact and inner-loop fluctuations caused by the clearances and backlash are essentially eliminated. The

TABLE III
MAXIMUM ERRORS IN THE LOAD EXPERIMENTS

	Load condition			
	miniclosed FOC	miniclosed DB-PCC	semiclosed k_d=40	semiclosed k_d=70
$[\text{rad}]$ $\theta_c^* - \theta_c$	0.1166	0.1093	0.0755	0.0582
$[\text{rad}/s]$ $\dot{\theta}_c^* - \dot{\theta}_c$	0.4835	0.4805	-0.4840	0.2295

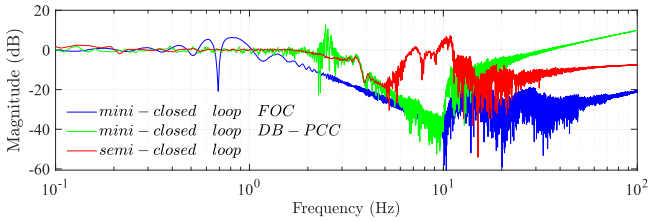

Fig. 15. Bandwidth comparison.

overall smoothness of speed, current, and torque in the proposed semiclosed-loop approaches the control effect of the miniclosed loop. These results in reduced impacts and mechanical collision forces. In scenarios where the control effect of the inner-loop waves for SPMSM in the semiclosed loop is even close to that of the miniclosed loop, there is a significant improvement in the error tracking angle of the crank. This represents a clear and notable performance enhancement.

The results, the control precision of the press machine's crankshaft is greatly improved, and the waveform of the machine's current control approaches that of the miniclosed loop. Due to the reduced switching frequency caused by using FCS-PCC, there is still some level of current harmonics.

In the four sets of experiments under heavy-load conditions, considering the precision of position and speed control during the motion process as well as the average error, the performance of the semiclosed-loop control with $k_d = 70$ still demonstrates the best trajectory tracking capability in Table III. In comparison between semiclosed loop and miniclosed-loop control, apart from when the crank position approaches π, the smoothness of machine current and torque curves in the semiclosed-loop control remains very close to the effect of the miniclosed loop.

As the crank approaches the vicinity of the BDC during motion, the reactive force of the load spring is at its maximum. In the semiclosed-loop control algorithm, the current remains relatively high at this point. Thanks to FOC relying on PI error accumulation for a long time, the miniclosed loop gradually reduces the output current when the machine is stationary. In contrast, semiclosed loop control relies on the real-time error to the output electromagnetic torque, requiring a larger current to overcome the resistance.

By analyzing the control methods in the frequency domain, it can be obtained from a bode diagram of the crank position the miniclosed-loop bandwidth with FOC and DB-PCC are 1.09 Hz and 2.15 Hz, respectively. However, the position bandwidth of the proposed method is 2.4 Hz. In Fig. 15, the results show that the position control of the proposed method can also achieve

TABLE IV
SWITCHING FREQUENCY OF THE PROPOSED METHOD

	0–1s	1–2s	2–3s	3–4s
No-load condition	2315	2686	1957	2451
Load condition	2291	2618	2117	2360

better dynamic performance at a higher frequency. The position response of the miniclosed loop with FOC and DB-PCC sharply deteriorates at 0.69 Hz and 2.27 Hz.

The reason is that in the cascaded structure of the miniclosed loop, the current reference value is essentially obtained by accumulating the speed control loop error and using traditional three-loop PI control. However, the proposed semiclosed-loop control approach mentioned in the article directly calculates the machine output torque using feedback values such as position and speed errors and feed-forward values such as acceleration reference, significantly increasing the bandwidth. This method no longer relies on error accumulation for adjustment but employs real-time error and a feed-forward structure for current online regulation.

The semiclosed method proposed also reduces the large number of switching frequencies compared to the 10-kHz sampling frequency and 20-kHz switching frequency in FOC in Table IV. The results show that it saves much more energy during the IGBT switch.

V. CONCLUSION

The proposed control algorithm, which combines computed torque and MPC, has notably improved the bandwidth of system response. This advancement has resulted in a substantial enhancement in the position and speed accuracy of the servo press crank, under both no-load and heavy-load conditions, by an order of magnitude. The analysis of the control parameters reveals that the speed parameter k_d has a dual effect: It not only influences the speed-tracking error but also plays a direct role in mitigating the position-tracking error. Furthermore, the switching frequency is decreased by three-quarters. Lower switching frequency will save energy in practical industrial applications. Hence, the method is provided, which theoretical and experimental analyses have confirmed, showcasing its superiority in both press performance and electrical drive control. In the forthcoming period, ongoing efforts will be made to advance novel algorithms to further diminish position errors, specifically at the BDC. This endeavor is expected to enhance the overall quality of the formation process.

REFERENCES

[1] R. Halicioglu, L. C. Dulger, and A. T. Bozdana, "Structural design and analysis of a servo crank press," *Eng. Sci. Technol., Int. J.*, vol. 19, no. 4, pp. 2060–2072, 2016.
[2] J. Olaizola, C.-S. Bouganis, E. S. De Argandoña, A. Iturrospe, and J. M. Abete, "Real-time servo press force estimation based on dual particle filter," *IEEE Trans. Ind. Electron.*, vol. 67, no. 5, pp. 4088–4097, May 2019.
[3] K. Kawamoto, H. Ando, and K. Yamamichi, "Application of servo presses to metal forming processes," *Procedia Manuf.*, vol. 15, pp. 31–38, 2018.
[4] J. Olaizola et al., "Integral design and manufacturing methodology of a reduced-scale servo press," *IEEE/ASME Trans. Mechatronics*, vol. 26, no. 5, pp. 2418–2428, Oct. 2021.

[5] A. Jomartov et al., "Dynamic model of servo mechanical press," in *Proc. Symp. Robot Des., Dyn., Control*, 2020, pp. 170–178.
[6] J. Gao, S. Zhao, F. Jiang, W. Du, and Z. Zheng, "A novel hollow two-sided output PMSM integrated with mechanical planetary gear: A solution for drive and transmission system of servo press," *IEEE/ASME Trans. Mechatronics*, vol. 27, no. 5, pp. 3076–3086, Oct. 2022.
[7] W. Lu, Z. Zhang, K. Ji, D. Wu, J. Lin, and J. Qian, "Research on short time and heavy load driving system of crank servo press based on feedforward and decoupling control," *Adv. Mech. Eng.*, vol. 10, no. 3, 2018, Art. no. 1687814018767185.
[8] Q. Li, Q. Chen, J. Gao, A. Li, H. Li, and R. Kennel, "Application of hybrid model predictive control for servo press," in *Proc. IEEE Int. Conf. Predictive Control Elect. Drives Power Electron.*, 2021, pp. 426–431.
[9] X. Chen, S. Gao, and T. Wang, "Experimental verification of dynamic behavior for multi-link press mechanism with 2D revolute joint considering dry friction clearances and lubricated clearances," *Nonlinear Dyn.*, vol. 109, no. 2, pp. 707–729, 2022.
[10] X. Chen, Y. Tang, and S. Gao, "Dynamic modeling and analysis of hybrid driven multi-link press mechanism considering non-uniform wear clearance of revolute joints," *Meccanica*, vol. 57, pp. 229–250, 2022.
[11] W. Kacalak, M. Majewski, and Z. Budniak, "Innovative design of non-backlash worm gear drives," *Arch. Civil Mech. Eng.*, vol. 18, pp. 983–999, 2018.
[12] Z. Zhou and R. Guo, "A disturbance-observer-based feedforward-feedback control strategy for driveline launch oscillation of hybrid electric vehicles considering nonlinear backlash," *IEEE Trans. Veh. Technol.*, vol. 71, no. 4, pp. 3727–3736, Apr. 2022.
[13] T.-C. Li, C.-C. Kuo, C.-Y. Yang, K.-W. Liu, P.-H. Li, and B.-T. Lin, "Influence of motion curve errors of direct-drive servo press on stamping properties," *Int. J. Adv. Manuf. Technol.*, vol. 120, no. 7/8, pp. 4461–4476, 2022.
[14] T. Wang, G. Luo, Z. Chen, W. Tu, and C. Liu, "An improved robust model predictive speed control with inertia identification for PMSM drives in electro-hydrostatic actuator," *IEEE Trans. Power Electron.*, vol. 38, no. 11, pp. 13825–13841, Nov. 2023.
[15] Q. Hou and S. Ding, "Finite-time extended state observer-based super-twisting sliding mode controller for PMSM drives with inertia identification," *IEEE Trans. Transp. Electrific.*, vol. 8, no. 2, pp. 1918–1929, Jun. 2022.
[16] Y. Chen, M. Yang, J. Long, W. Qu, D. Xu, and F. Blaabjerg, "A moderate online servo controller parameter self-tuning method via variable-period inertia identification," *IEEE Trans. Power Electron.*, vol. 34, no. 12, pp. 12165–12180, Dec. 2019.
[17] M. Yang, Q. Ni, X. Liu, and D. Xu, "Vibration suppression and over-quadrant error mitigation methods for a ball-screw driven servo system with dual-position feedback," *IEEE Access*, vol. 8, pp. 213758–213771, 2020.
[18] P. Guan, J. Ou, and J. Zhang, "Full closed loop algorithm of position and torque double loop control based on linear active disturbance rejection," in *Proc. 26th Int. Conf. Elect. Mach. Syst.*, 2023, pp. 4585–4589.
[19] H. Liu, Y. Wang, and X. Shan, "Full closed loop-based dynamic accuracy enhancement for elastic joints," *J. Power Electron.*, vol. 22, no. 6, pp. 959–969, 2022.
[20] Y. Lin, D.-D. Chen, M.-S. Chen, X.-M. Chen, and J. Li, "A precise BP neural network-based online model predictive control strategy for die forging hydraulic press machine," *Neural Comput. Appl.*, vol. 29, pp. 585–596, 2018.
[21] R. Halicioglu, L. C. Dulger, and A. T. Bozdana, "Modeling, design, and implementation of a servo press for metal-forming application," *Int. J. Adv. Manuf. Technol.*, vol. 91, no. 5, pp. 2689–2700, 2017.
[22] Q. Li, J. Gao, Q. Wang, and R. Kennel, "Model predictive torque control of induction motor drives with computed torque for servo press," in *Proc. IEEE 9th Int. Power Electron. Motion Control Conf.*, 2020, pp. 3063–3067.
[23] Q. Li, Y. Lv, R. Kennel, and J. Rodriguez, "Model predictive control of PMSM with computed torque for servo press," in *Proc. IEEE Int. Conf. Predictive Control Elect. Drives Power Electron.*, 2023, pp. 1–7.
[24] Q. Li, H. Li, J. Gao, Y. Xu, J. Rodriguez, and R. Kennel, "Nonlinear-disturbance-observer-based model-predictive control for servo press drive," *IEEE Trans. Ind. Electron.*, vol. 71, no. 8, pp. 8448–8458, Aug. 2024.
[25] L. Ge, J. Zhong, Q. Cheng, Z. Fan, S. Song, and R. D. Doncker, "Model predictive control of switched reluctance machines for suppressing torque and source current ripples under bus voltage fluctuation," *IEEE Trans. Ind. Electron.*, vol. 70, no. 11, pp. 11013–11021, Nov. 2023.
[26] E. Zafra, S. Vazquez, T. Geyer, R. P. Aguilera, and L. G. Franquelo, "Long prediction horizon FCS-MPC for power converters and drives," *IEEE Open J. Ind. Electron. Soc.*, vol. 4, no. 1, pp. 159–175, May 2023.
[27] M. F. Elmorshedy, W. Xu, F. F. El-Sousy, M. R. Islam, and A. A. Ahmed, "Recent achievements in model predictive control techniques for industrial motor: A comprehensive state-of-the-art," *IEEE Access*, vol. 9, pp. 58170–58191, 2021.
[28] X. Zhang, C. Zhang, C. Xu, and S. Fan, "Multi-mode model predictive control for PMSM drive system," *IEEE Trans. Transp. Electrific.*, vol. 9, no. 1, pp. 667–677, Mar. 2023.
[29] Y. Chen, C. Liu, H. Wen, and Z. Dong, "Improved model predictive control for multi-motor system using reduced-switch-count VSI with current minimization," *IEEE Trans. Power Electron.*, vol. 38, no. 7, pp. 8786–8797, Jul. 2023.
[30] F. Wang, L. He, J. Kang, R. Kennel, and J. Rodríguez, "Adaptive model predictive current control for PMLSM drive system," *IEEE Trans. Ind. Electron.*, vol. 70, no. 4, pp. 3493–3502, Apr. 2023.
[31] C. Ma, J. Rodriguez, C. Garcia, and F. D. Belie, "Integration of reference current slope based model-free predictive control in modulated PMSM drives," *IEEE Trans. Emerg. Sel. Topics Power Electron.*, vol. 11, no. 2, pp. 1407–1421, Apr. 2023.
[32] H. Lin, S. Niu, Z. Xue, and S. Wang, "A simplified virtual-vector-based model predictive control technique with a control factor for three-phase SPMSM drives," *IEEE Trans. Power Electron.*, vol. 38, no. 6, pp. 7546–7557, Jun. 2023.
[33] H. Kawai, Z. Zhang, R. Kennel, and S. Doki, "Direct speed control based on finite control set model predictive control with voltage smoother," *IEEE Trans. Ind. Electron.*, vol. 70, no. 3, pp. 2363–2372, Mar. 2023.
[34] T. Wang, G. Luo, C. Liu, Z. Chen, and W. Tu, "Speed control for variable speed PMSM drive system using nonlinear variable-horizon predictive functional control," *IEEE Trans. Emerg. Sel. Topics Power Electron.*, vol. 11, no. 2, pp. 1454–1465, Apr. 2023.
[35] Z. Sun, S. Xu, G. Ren, C. Yao, and G. Ma, "A cascaded band based model predictive current control for PMSM drives," *IEEE Trans. Ind. Electron.*, vol. 70, no. 4, pp. 3503–3514, Apr. 2023.
[36] Q. Li, H. Li, J. Gao, and R. Kennel, "Model predictive control using the singular perturbation theory for permanent-magnet synchronous machines," *IEEE Trans. Power Electron.*, vol. 39, no. 3, pp. 3533–3543, Mar. 2024.

Qi Li (Graduate Student Member, IEEE) was born in Shandong, China, in 1986. He received the B.E. degree in automation engineering from Qingdao University, Qingdao, China, in 2008, and the M.E. degree in automation engineering from the Beijing University of Technology, Beijing, China, in 2011. He is currently working toward the Ph.D. degree in electrical drive with the Institute for High-Power Converter Systems, Technical University of Munich, Munich, Germany.

From 2011 to 2018, he was an Engineer to develop electrical drives for electric vehicles, electrical drive, power electronics, construction machinery, and servo motors in China. His research interests include electrical drives, predictive control, nonlinear control, and servo press.

Yan Lv was born in Hubei, China, in 1953. He received the B.E. and master's degrees in mechanical engineering from the Huazhong University of Science and Technology, Wuhan, China, in 1976 and 1987, respectively, and the Dr.-Ing. degree in mechanical engineering from the Nippon Institute of Technology, Tokyo, Japan, in 1992.

From 1993 to 2014, he was the Minister of R&D and Executive Director with Amino Corporation, Ltd., Japan, for research and development of stamping equipment. Since 2015, he was been a Full Chief Expert with Jining Keli Photoelectronic Industrial Company, Ltd., Jining, China. His research interests include mechanical design, servo press, metal forming, and control system.

Ralph Kennel (Senior Member, IEEE) was born in Kaiserslautern, Germany, in 1955. He received the Diploma and Dr.-Ing. (Ph.D.) degrees in electrical engineering from the University of Kaiserslautern, Kaiserslautern, in 1979 and 1984, respectively.

From 1983 to 1999, he worked in several positions with Robert BOSCH GmbH, Germany. Until 1997, he was responsible for the development of servo drives. He was one of the main supporters of VECON and SERCOS interface, two multicompany development projects for a microcontroller and a digital interface especially dedicated to servo drives. Furthermore, he took actively part in the definition and release of new standards with respect to CE marking for servo drives. Between 1997 and 1999, he was responsible for Advanced and Product Development of Fractional Horsepower Motors in automotive applications. His main activity was preparing the introduction of brushless drive concepts to the automotive market. From 1994 to 1999, he was a Visiting Professor with the University of Newcastle-upon-Tyne, U.K. From 1999 to 2008, he was a Professor of Electrical Machines and Drives with Wuppertal University, Germany. He was an Extraordinary Professor with the University of Stellenbosch, South Africa, from 2016 to 2019 and a Visiting Professor with Haixi Institute, Chinese Academy of Sciences, from 2016 to 2021. Since 2008, he has been a Professor for Electrical Drive systems and Power Electronics with Technische Universitaet Muenchen, Munich, Germany. His main research interests include sensorless control of ac drives, predictive control of power electronics, and hardware-in-the-loop systems.

Dr. Kennel is a Fellow of IET (former IEE) and a Chartered Engineer in the U.K. Within IEEE, he is a Treasurer of the Germany Section as well as the Distinguished Lecturer of the Power Electronics Society (IEEE-PELS). He is a recipient of the Harry Owen Distinguished Service Award from IEEE-PELS in 2013, the EPE Association Distinguished Service Award in 2015, the 2019 EPE Outstanding Achievement Award, and the Doctoral degree honoris causa from Universitatea Stefan cel Mare, Suceava, Romania, in 2018.

Jose Rodriguez (Life Fellow, IEEE) received the Engineering degree in electrical engineering from the Universidad Tecnica Federico Santa Maria, Valparaiso, Chile, in 1977, and the Dr.-Ing. degree in electrical engineering from the University of Erlangen, Erlangen, Germany, in 1985.

Since 1977, he has been with the Department of Electronics Engineering, Universidad Tecnica Federico Santa Maria, where he was a Full Professor and the President. From 2015 to 2019, he was the President of Universidad Andres Bello, Santiago, Chile. Since 2022, he has been the President of Universidad San Sebastian, Santiago, Chile. He has coauthored 2 books, several book chapters, and more than 700 journal and conference papers. His main research interests include multilevel inverters, new converter topologies, control of power converters, and adjustable-speed drives.

Dr. Rodriguez is a recipient of a number of best paper awards from journals of the IEEE. He is a member of the Chilean Academy of Engineering. He is also a recipient of the National Award of Applied Sciences and Technology from the government of Chile and the Eugene Mittelmann Award from the Industrial Electronics Society of the IEEE in 2015. From 2014 to 2022, he was included in the list of Highly Cited Researchers published by Web of Science.